Can. J. Remote Sensing, Vol. 30, No. 3, pp. 424–436, 2004

Analysis of RADARSAT-1 data for offshore monitoring activities in the Cantarell Complex, Gulf of Mexico, using the unsupervised semivariogram textural classifier (USTC)

Fernando Pellon de Miranda, Arturo Mendoza Quintero Marmol, Enrico Campos Pedroso, Carlos Henrique Beisl, Pamela Welgan, and Luis Medrano Morales

Abstract. Understanding the temporal dynamics and spatial distribution of natural seepage phenomena in the Gulf of Mexico is fundamental for the definition of proper environmental management practices in this often cloud-covered region. RADARSAT-1 images analyzed in this paper were acquired using the wide 1 and wide 2 (W1, W2) and ScanSAR narrow 1 (SCN1) beam modes. Image processing was carried out using the unsupervised semivariogram textural classifier (USTC). In combination with RADARSAT-1 satellite images, and essential ancillary data, this technology enhances the detection of seepage slicks on the ocean surface based on radar texture. USTC classification of RADARSAT-1 data provided systematic evidence from space of the presence of prolific, present-day petroleum generation and migration in the Cantarell Complex of oil fields.

Résumé. La connaissance de la dynamique temporelle et de la répartition spatiale des phénomènes naturels de suintement dans le Golfe du Mexique est fondamentale dans l'élaboration des pratiques de gestion environnementale appropriées dans cette zone souvent recouverte de nuages. Les images RADARSAT-1 analysées dans cet article ont été acquises dans les modes à faisceau Large 1 et 2 (W1, W2) et ScanSAR à faisceau étroit (SCN1). Le traitement des images a été réalisé au moyen de la technique USTC (« unsupervised semivariogram textural classifier »). Cette technologie, basée sur la combinaison des images satellitaires de RADARSAT-1 et des données auxiliaires essentielles, facilite la détection des nappes de suintement à la surface de l'océan à partir de la texture radar. La classification USTC des données RADARSAT-1 a fourni une preuve systématique à partir de l'espace de l'existence d'un phénomène de génération et de migration prolifique et actuel de pétrole dans le Complexe Cantarell des champs de pétrole.
[Traduit par la Rédaction]

Introduction

Natural oil and gas seeps have historically provided invaluable information to oil explorers in frontier areas. First and foremost, seeps indicate the presence of generative hydrocarbon source rocks, without which there can be no accumulations. Mexican exploration activities in the Gulf of Mexico began soon after a fisherman, Mr. Cantarell, reported oil seeps in Campeche Bay. The complex of oil fields later discovered beneath the seeps was subsequently named after him. At present, Cantarell is the most important area for oil production in North America. It is interesting to note that oil seeps have been known in the southern Gulf of Mexico since pre-Colombian times. They were referred to as *chapopoteras* in the native dialect.

Important fisheries and delicate ecosystems surround this offshore region, making it highly sensitive to the presence of oil. In this context, an understanding of the temporal dynamics and spatial distribution of natural seepage phenomena is fundamental for the definition of proper environmental management practices. PEMEX Exploración y Producción is, therefore, in search of cutting-edge remote sensing technology from space to characterize oil seeps in the area of the Cantarell Complex. This initiative will allow improvement of the relationship between PEMEX Exploración y Producción and environmental authorities and society as a whole.

The offshore study area of Campeche Bay is often cloud covered. Spaceborne synthetic aperture radar (SAR) systems such as RADARSAT-1 are therefore ideal for this application,

Received 18 February 2003. Accepted 30 January 2004.

F.P. Miranda.[1] PETROBRAS Research and Development Center (PETROBRAS/CENPES), Avenida 1, Quadra 7, Cidade Universitária, Ilha do Fundão, CEP 21491-598, Rio de Janeiro, Brazil.

A.M.Q. Marmol and L.M. Morales. PEMEX Exploración y Producción, Región Marina Noreste (PEP/RMNE), Estudios Ambientales, Calle 25, No. 48, Col. Guadalupe, Cd. Del Carmen, Campeche, C.P. 24130, Mexico.

E.C. Pedroso and C.H. Beisl. RADARSAT Resource Centre in Brazil (CBRR), Universidade Federal de Rio de Janeiro (COPPE/UFRJ), Centro de Tecnologia, Bloco I-114, Cidade Universitária, Ilha do Fundão, CEP 21949-900, Rio de Janeiro, Brazil.

P. Welgan. RADARSAT International Inc., 13800 Commerce Parkway, Richmond, BC V6V 2J3, Canada.

[1]Corresponding author (e-mail: fmiranda@cenpes.petrobras.com.br).

since these systems are not affected by clouded conditions. Remote detection of natural seepage using spaceborne SAR has been successful in the Gulf of Mexico, as described by MacDonald et al. (1996), Scantland and Biegert (1996), and Biegert et al. (1997).

The significance of natural seepage to environmental monitoring in Campeche Bay has led PEMEX Exploración y Producción to use a technology developed by the PETROBRAS Research & Development Center (CENPES), in collaboration with RADARSAT International Inc. (RSI) and the RADARSAT Resource Centre in Brazil (CBRR – COPPE/UFRJ). In combination with RADARSAT-1 satellite images and essential ancillary data, this technology enhances the detection of natural oil slicks on the ocean surface.

A pilot project was conducted in 1997 in the deep-water mouth of the Amazon River, offshore Pará and Amapá states, northern Brazil (Miranda et al., 1998b). The result of this project was a fully developed image processing procedure, the unsupervised semivariogram textural classifier (USTC). The USTC is used to identify potential natural oil slicks based on sea-surface radar texture. The results of the pilot project were presented at the International Demonstration and Product Development subprogram of the Application Development and Research Opportunity (ADRO) program, and in 1998 the paper received the Canadian Space Agency (CSA) and RSI ADRO Merit Award for Most Promising Commercial Application, attesting to the potential of this technology.

Oil detection using SAR

The physical mechanism that allows detection of oil seeps and spills is the dampening of capillary waves present on the ocean surface. These capillary waves, which are only a few centimetres in length, produce backscattering of the incident radar pulse owing to a Bragg scattering mechanism (Johannessen et al., 1994). As a result, ocean regions containing oil are dark in contrast with the background radar signal (clutter).

Although SAR images can be very useful for oil detection in the sea, several other ocean-surface phenomena can also produce regions of low radar backscatter that, in turn, can lead to misinterpretation (Fingas and Brown, 1997; Fu and Holt, 1982). These processes are (*i*) slicks caused by freshwater intrusions, mostly of riverine origin; (*ii*) regions of very weak or no wind; (*iii*) shadow zones of waves behind structures, islands, or land; (*iv*) beds of underwater vegetation that calm the surface waters; and (*v*) biogenic oils. The turbulence in a ship's stern wake will temporarily dampen any capillary waves, also resulting in low radar backscatter. Point target signatures such as those of ships, however, can often be recognized by shape (the position of the vessel's longitudinal axis can be determined in some cases). Releases of oil from offshore production and transportation facilities can also be mistakenly interpreted as natural oil slicks. Oil platforms are characterized as strong bright points in RADARSAT-1 images (Espedal and Johannessen, 2000). Oil spills also originate from releases from ships, e.g., during cleaning of oil tanks.

Particular sea state conditions are also known to limit the usefulness of SAR images for oil seep detection. Very weak winds do not produce sufficient sea clutter in the areas surrounding the oil seep to give the backscatter sufficient contrast for observing a slick. Very strong winds can produce too much turbulence or waves on the surface layer of the ocean, hindering detection, and tall waves in heavy seas prevent radar detection in the wave trough. The range of wind velocity considered ideal for oil detection using SAR lies between 3 and 8 $m \cdot s^{-1}$ (Staples and Hodgins, 1998). Further, heavy rain on the ocean surface produces turbulence that weakens capillary waves. This results in an area of low radar backscatter in the center of the rain cell and an area of higher scattering in the surrounding areas (Johannessen et al., 1994). As a result, regions containing heavy rain cells make oil seep detection very difficult indeed. This phenomenon is especially problematic in tropical regions such as the Gulf of Mexico.

Another important factor to be considered in the interpretation of SAR images is that the contrast between oil seeps and their surroundings largely depends on the incidence angle of the radar beam. Steep incidence angles (10°–40°) improve the detection of oil seeps (e.g., extended low 1, standard 1 to standard 4, wide 1 to wide 2, and ScanSAR narrow 1 RADARSAT-1 beam modes). The discrimination capability also depends on the oil seep size and on the resolution of the chosen RADARSAT-1 beam mode. RADARSAT-1 images in the wide 1 (W1) beam mode are preferable when used in oil seep detection because they provide a cost-effective compromise between nominal area coverage (165 km × 165 km), incidence angle range (20°–31°), and nominal resolution (30 m). ScanSAR narrow 1 (SCN1) images are often used because they provide a synoptic view of offshore study areas. This beam mode is characterized by nominal area coverage of 300 km × 300 km, incidence angle ranging from 20° to 40°, and nominal resolution of 50 m.

It can be seen, then, that the success of RADARSAT-1 in detecting an oil seep is a function not only of the beam mode and position, but also of the environmental and weather conditions prevailing on the image acquisition date. Therefore, oceanic and meteorological ancillary data and derived analysis were integrated in this study to aid in the selection and interpretation of the RADARSAT-1 images.

Study area

The site of investigation is situated in the continental shelf of Campeche State and constitutes the largest petroleum province in the Gulf of Mexico (**Figure 1**). The presence of a prominent offshore oil seep about 70 km north of Ciudad del Carmen aided PEMEX in defining the location of the first exploratory well in the region (Chac-1). The structure drilled in 1976 at Chac-1 became part of the Cantarell oil field.

Oil seepage in Cantarell occurs primarily in shallow water areas of salt tectonics and active petroleum generation from

source rocks of Tithonian (Upper Jurassic) age, where faults and salt diapirs penetrate overlying sediments and create migration pathways, either from source rock or reservoir, to the sea floor.

The tectonic provinces of Campeche Bay are shown in **Figure 2**. The main geologic characteristics of these provinces are as follows:

(1) Saline Offshore Basin — This province is the offshore continuation of the Isthmian Saline Basin. Salt deposits that flowed and produced diapirs, domes, turtle structures, canopies, salt walls, and salt tongues constitute the Saline Offshore Basin. The basin includes the hydrocarbon accumulations of the Marbella area, which are associated with salt diapirs.

(2,3) Comalcalco and Macuspana offshore basins — These Miocene–Pliocene basins form major extensional zones associated with down-to-basin, listric normal faults. These faults have a Middle Miocene shaly horizon as a detachment surface.

(4) Yucatán Platform — This province includes the Yucatán Peninsula and the adjoining carbonate bank. It acted as a

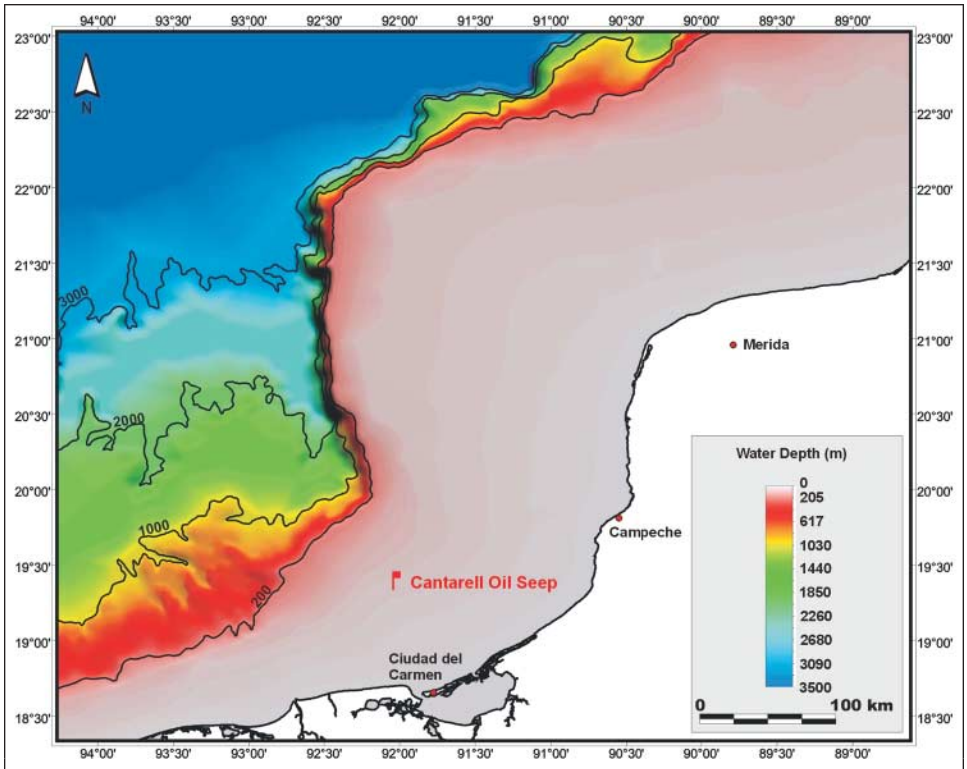

Figure 1. Location map of the Cantarell oil seep.

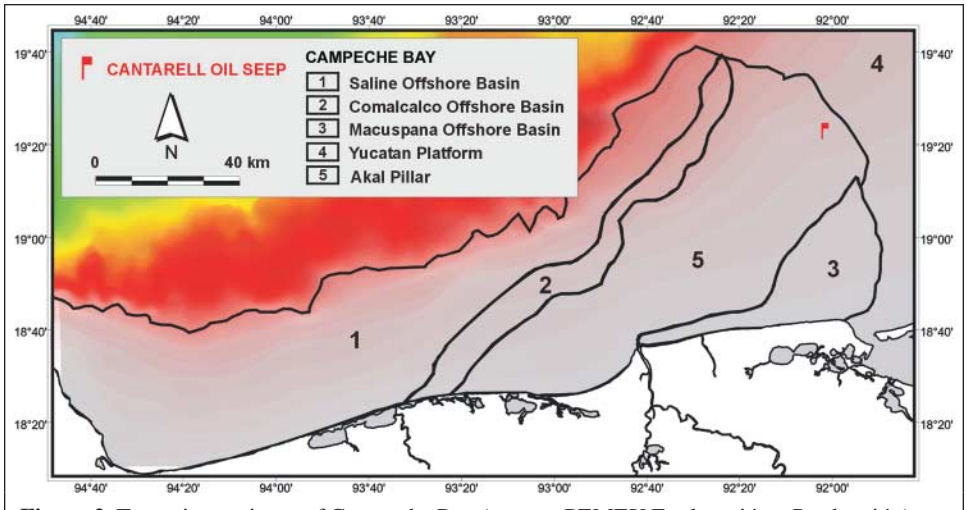

Figure 2. Tectonic provinces of Campeche Bay (source: PEMEX Exploración y Producción).

rigid block during the tectonic evolution of the Gulf of Mexico.

(5) Akal Pillar — This province is the offshore extension of the "Villahermosa Uplift", which lies between the Comalcalco and Macuspana offshore basins. The slope zone of the Yucatán Platform defines its northeastern limit. Salt tectonics played an important role in defining the structural framework of major oil fields such as Cantarell.

The seismic structural map at the top of the Upper Cretaceous – Lower Paleocene bank edge talus (Akal Pillar region) is included in this study as part of the ancillary information necessary to define the geologic control of the oil slicks highlighted in the RADARSAT-1 images (**Figure 3**). Thrust faults oriented in the northwest–southeast direction are the main structural features in the Cantarell region. They are associated with northwest–southeast-trending folds, asymmetric or overturned to the northeast (not shown in **Figure 3**).

Criteria for selection of RADARSAT-1 images

RSI offers the RADARSAT Offshore Exploration Service (OES), which has been developed for applications requiring weather-dependent SAR imagery (e.g., oil seep detection). The OES includes the option of meteorological programming at a reduced price. Meteo programming allows the choice of one scene to be processed for a given area from three imaging attempts, using weather conditions at the time of acquisition as the deciding factor. In this study, 12 RADARSAT-1 W1 images were selected for processing in 2000 from a possible 36 attempts from June to December. In addition, 20 SCN1, W1, or W2 images were selected for processing in 2001 out of a possible 60 potential acquisition dates from April to December. Ancillary oceanic and meteorological data and derived analysis were used to choose the suitable image from the three attempts for final processing and interpretation. Therefore, data from the National Oceanic and Atmospheric Administration (NOAA), geostationary operational environmental satellite (GOES-8), QuikSCAT, and ocean topography experiment Poseidon

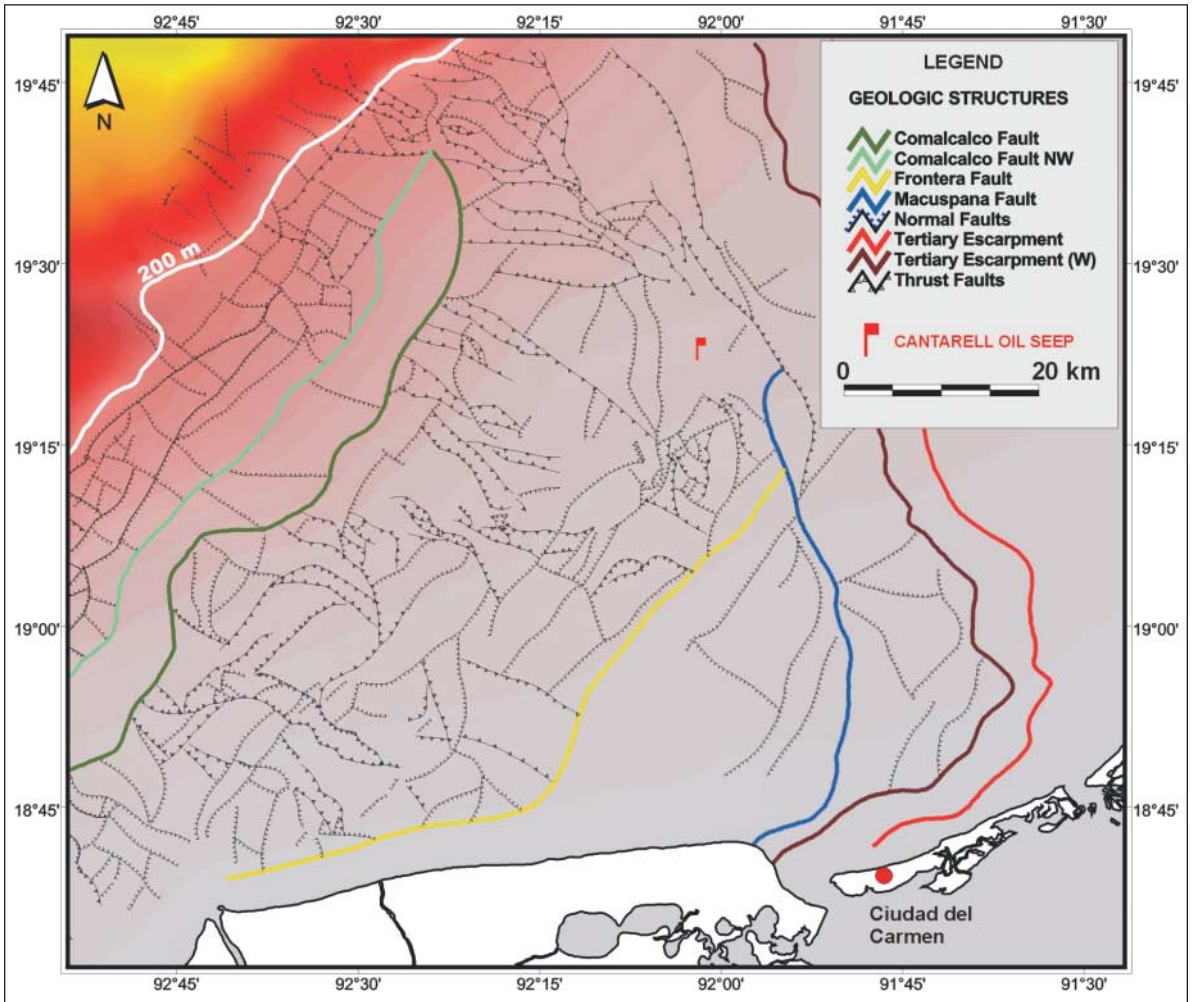

Figure 3. Seismic structural map at the top of the Upper Cretaceous – Lower Paleocene bank edge talus (Akal Pillar region) (source: PEMEX Exploración y Producción).

(TOPEX-Poseidon) satellites were used to provide information about the environmental conditions at the time of potential image acquisition dates in the SCN1, W1, and W2 operational beam modes. These oceanographic and meteorological value-added products are described as follows:

(1) Advanced very high resolution radiometer (AVHRR) data processing for generation of sea surface temperature (SST) maps — The AVHRR is a five-channel sensor installed on board NOAA satellites and acquires one visible band (band 1), one reflected infrared band (band 2), and three thermal infrared bands (bands 3, 4, and 5), all with a spatial resolution of 1.1 km × 1.1 km. AVHRR data are processed in this study for the generation of SST maps. The oceanographic interpretation of the temperature maps provides a synoptic view of the SST field and furnishes relevant information about important features such as upwelling, oceanic fronts, and position and meandering patterns of oceanic currents. AVHRR images are obtained as close as possible to the time of the RADARSAT-1 data acquisition. A joint analysis of RADARSAT-1 and AVHRR images is carried out whenever necessary to identify the main oceanographic features present in both products. This procedure aids in the interpretation of the RADARSAT-1 images for the detection of oil seeps.

(2) Heavy rain maps — Oceanic areas under the effect of heavy rainfall cannot be used in SAR images for oil seep detection. One possible form of estimating the location of such regions is through monitoring of highly developed cumulonimbus cloud systems. These clouds have extremely low top temperatures (lower than –50 °C) because of their very large vertical extent. Temperature values can be calculated (**Table 1**) using data acquired by the sensor imager installed on board the GOES-8 satellite. The imager instrument consists of five channels ranging from the visible to the thermal infrared region of the electromagnetic spectrum. The visible channel has a resolution of 1 km, and most of the infrared channels have a resolution of 4 km at nadir. Therefore, thermal infrared images from the GOES imager were used to highlight these low-temperature values at cloud tops, resulting in the generation of maps containing possible heavy rain cell areas.

(3) Ocean wind pattern — Knowledge of the magnitude of oceanic winds is important to assess the usefulness of SAR images for natural oil seep detection. Ideal wind velocity conditions range from 3.0 to 8.0 $m \cdot s^{-1}$ (Staples and Hodgins, 1998) (**Table 1**). Data were retrieved from the SeaWinds instrument on board the QuikSCAT satellite. This scatterometer is an all-weather microwave radar sensor that measures near-surface wind speed and direction. The swath width during each orbit is 1800 km. The instrument collects data over ocean, land, and ice and covers 90% of the earth's surface in 1 day. SeaWinds measures wind speed from 3.0 to 20.0 $m \cdot s^{-1}$ with an accuracy of 2.0 $m \cdot s^{-1}$ in intensity and 20° in direction. The wind vector resolution is 0.5°.

(4) Wave pattern — Wave height information was obtained with the aid of an altimeter sensor on board the TOPEX-Poseidon satellite. This instrument sends a radar pulse to the ocean surface that is reflected back to the antenna. Significant wave height values are extracted from the altimeter data based on the slope of the edge of the altimeter waveform. A calm sea with low waves returns a short, sharply defined pulse. A rough sea with high waves returns a stretched pulse. Sea state conditions suitable for oil seep detection are characterized by wave heights of less than 1.5 m (**Table 1**).

Table 1. Recommended parameter intervals for oil detection using SAR.

Parameter	Instrument	Satellite	Recommended interval
Cloud top temperature of rain cells (°C)	Imager	GOES-8	< –50
Wind velocity ($m \cdot s^{-1}$)	SeaWinds	QuikSCAT	3.0–8.0
Wave height (m)	Altimeter	TOPEX-Poseidon	<1.5

Textural classification of RADARSAT-1 images

Reliance on spatial structure for remote sensing data classification is useful when the textural characteristics of an image are more important than its spectral information content. In the case of a single-frequency/single-polarization spaceborne radar system such as RADARSAT-1 (C-band/HH polarization), it is appropriate to choose a classifier that considers a pixel value in the context of its nearest neighbors. One way to carry out this approach is to examine image texture using the semivariogram function (Miranda and MacDonald, 1989; Rubin, 1989).

The semivariogram textural classifier (STC) proposed by MacDonald (1991) was the first algorithm to perform image classification based on the semivariogram signature of remote sensing data. Application of semivariograms for classification of spaceborne radar images includes (*i*) terrain recognition using Magellan and SIR-C data (Carr, 1996; Carr and Miranda, 1998), (*ii*) vegetation mapping in rainforest regions using SIR-B and JERS-1 SAR data (Miranda, 1990; Miranda et al., 1992; 1996; 1998a; Miranda and Carr, 1994), and (*iii*) land-use mapping in urban areas using SIR-C data (Carr and Miranda, 1998).

The STC classification of JERS-1 SAR images obtained over the Amazon rainforest yielded compelling, albeit not completely accurate results, since a large percentage of pixels were labeled as unclassified. To circumvent such a problem, textural classes were defined by Miranda et al. (1997) in an

unsupervised fashion, followed by postclassification interactive class aggregation. The chosen classification algorithm was the USTC, which was subsequently used by Miranda et al. (1998b; 1998c; 1998d) to identify potential natural oil slicks based on sea-surface radar textures in the deep-water mouth of the Amazon River. This classifier was also successfully used to identify mesoscale oceanic features in the offshore Campos Basin, southeastern Brazil (Beisl et al., 2000), and to highlight oil-covered areas on the water surface during the Guanabara Bay spill, Rio de Janeiro, Brazil (Bentz et al., 2000; Bentz and Miranda, 2001).

The USTC was applied in this study to RADARSAT-1 SCN1, W1, and W2 data to enhance ocean surface features. It is a deterministic classifier that provides the option of combining both textural and radiometric information (Miranda et al., 1997). Radiometric information is conveyed by the despeckled digital number (DN_{dsp}) value. The speckle noise reduction algorithm to be used is the adaptive median filter (Fonseca, 1996). Textural information is described by the shape and value of the circular semivariogram function, which has the following form:

$$\gamma(x_0, h) = \frac{1}{2n} \sum_{\theta=0}^{2\pi} [DN(x_0 + r) - \mu_H(x_0)],$$

where $\gamma(x_0, h)$ is the semivariogram function at pixel location x_0 and radial lag distance of h pixels; $DN(x_0 + r)$ is the digital number value at radial lag distance r from x_0 (radius h, angle θ); $\mu_H(x_0)$ is the mean value of a circular neighborhood of radius H and center x_0; H is the maximum radial lag distance (in pixels) suitable to describe the data (we used $H = 6$ in this project); and n is the number of pixel neighbors at radial lag distance h.

Textural information is also described by the digital number variance (σ) in a circular neighborhood of radius H around the pixel [$\sigma^2_H(x_0)$]. The DN variance is included in the classification procedure because it reflects the value of the semivariogram function for a very large lag distance (greater than H).

For a pixel location x_0 in a RADARSAT-1 image, the vector $\boldsymbol{Z}(x_0)$, of dimension $H + 2$, has the following form:

$$\boldsymbol{Z}(x_0) = [DN_{dsp}(x_0),\ \gamma(x_0, 1), \gamma(x_0, 2), \ldots, \gamma(x_0, H), \sigma^2_H(x_0)].$$

The classification procedure is accomplished based on all components of this $H + 2$ dimensional vector, calculated for each pixel location. The ISODATA clustering algorithm is applied to carry out the unsupervised classification of this set of vectors. After the unsupervised classification, results obtained from the clustering program are merged together through interactive class aggregation (an aggregate is a grouping of one or more classes considered to be of thematic significance). In this study, class aggregation was performed to discriminate patches of smooth texture from rough to intermediate offshore areas of the RADARSAT-1 image. Raster polygons defining smooth surface regions related to potential natural oil slicks in the Cantarell area were then highlighted and subsequently isolated in vector format.

Verification of RADARSAT-1 and USTC performance using a controlled oil release

Operational monitoring of oil seeps in the marine environment can be facilitated by the systematic use of textural classification of RADARSAT-1 data. To verify the performance of oil detection using radar imagery and of the USTC algorithm for oil slick mapping, an experiment including a controlled release of oil was conducted by PEMEX Exploración y Producción on 23 November 2000, 2 h before the acquisition of a RADARSAT-1 scene. An ascending RADARSAT-1 W1 image was acquired on 24 November 2000 at 00:11:02 GMT (06:11:02 p.m. local time on 23 November 2000). The objective of this experiment was to demonstrate the capability of RADARSAT-1 to accurately map oil on the sea surface.

Under the supervision of Mexican authorities (Secretaría de Marina Armada de México (SEMAR)), two controlled oil spills were released from a ship; the volume involved was 100 L (approximately 0.63 barrels) and 476 L (approximately 3 barrels) of Mayan oil (21.9° American Petroleum Institute (API)). The distance between the two spills at the time of RADARSAT-1 W1 data acquisition was 1.85 km (**Figure 4**). The meteorological conditions were obtained at the ship 2 h before the RADARSAT-1 acquisition. Wind speed range was from 5.1 to 7.7 $m \cdot s^{-1}$, and wave height was less than 1.22 m. At the time of RADARSAT-1 acquisition, a neighboring vessel reported wind speeds ranging from 5.5 to 6.9 $m \cdot s^{-1}$ and wave heights between 0.6 and 1.2 m. These values reach the standards adopted in the present study for adequate wind and wave conditions regarding SAR detection of oil in the sea (**Table 1**). According to the SeaWinds instrument on board the QuikSCAT satellite, wind speed in the study area was ranging from 3.0 to 4.0 $m \cdot s^{-1}$ at the time of RADARSAT-1 acquisition; the altimeter sensor on board the TOPEX-Poseidon satellite indicated wave heights ranging from 0.5 to 1.5 m (**Table 3**). The USTC classification of the RADARSAT-1 W1 image allowed the identification and mapping of the oil slicks (features B and C in **Figure 4**; see also **Table 2**). This result attests to the potential of such a textural classification approach for operational monitoring of oil seeps in the marine environment.

Thematic maps of oil seeps in the Cantarell area

Data selection in the study area was performed based on the oceanographic and meteorological value-added products used to provide information about the environmental conditions at the time of potential RADARSAT-1 acquisition dates. As a result, 12 W1 images were chosen for processing in 2000. It is remarkable to note that seepage slicks in the Cantarell area were detected in nine out of the 12 selected W1 images

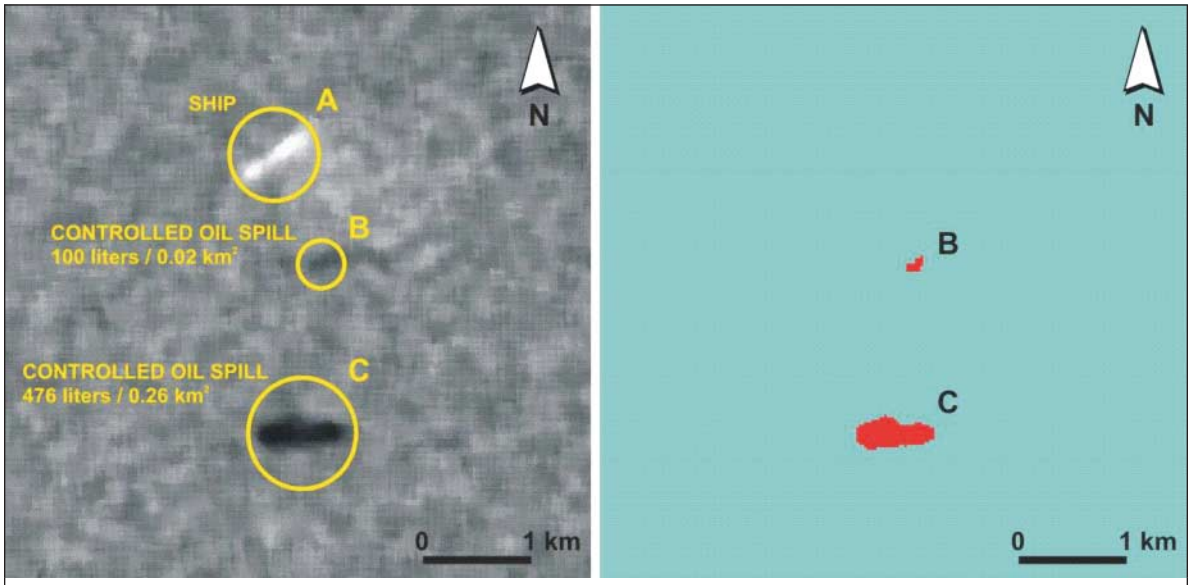

Figure 4. Detail of the original RADARSAT-1 W1 image (median filter processed) acquired on 23 November 2000, showing the ship (bright feature A) and the controlled spills (dark features B and C). Both controlled spills were successfully delineated using the USTC algorithm.

Table 2. Characteristics of the RADARSAT-1 W1 image expression of the controlled oil spills released on 23 November 2000 (18:11:02 local time).

Parameter	1° slick (100 L)	2° slick (476.28 L)
Central point in UTM coordinates (WGS-84)	2175561.896N, 596167.226E	2173656.896N, 595852.226E
Central point in geographic coordinates (WGS-84)	19°40′23.0″N, 92°4′57.2″W	19°39′21.1″N, 92°5′8.4″W
Area (km^2)	0.26	2.82
Perimeter (km)	0.02	0.72

Table 3. RADARSAT-1 images acquired in 2000 of seepage slicks in the Cantarell area.

Acquisition date (GMT)	Operational beam mode	Orbit	Wind velocity ($m \cdot s^{-1}$)[a]	Wave height (m)[b]	Rain cells[c]
10 June	W1	Descending	6.0–12.0	1.0–2.0	Not present
10 July	W1	Ascending	4.0–7.0	0.0–1.0	Not present
21 July	W1	Descending	3.0–7.0	1.0–2.0	Not present
28 July	W1	Descending	2.0–6.0	0.0–1.0	Not present
20 Aug.	W1	Ascending	4.0–6.0	0.5–1.5	Not present
21 Aug.	W1	Descending	8.0–10.0	1.0–1.5	Not present
14 Sept.	W1	Descending	2.0–4.0	0.5–1.5	Not present
07 Oct.	W1	Ascending	5.0–9.0	1.5–2.5	Not present
24 Nov.	W1	Descending	3.0–4.0	0.5–1.5	Not present

[a]QuikSCAT.
[b]TOPEX-Poseidon.
[c]GOES-8.

(**Table 3**). Cantarell seepage activity was recorded in 92% of images acquired. Such a result constitutes systematic evidence from space of the presence of prolific, present-day oil generation and migration in this part of Campeche Bay.

An impressive example of the spatial distribution of natural seepage phenomena in the Cantarell area is portrayed in the descending W1 image acquired on 28 July 2000 (**Figure 5**). The seepage slick identified by means of USTC classification occupied an area of 74.23 km^2.

As shown in **Table 3**, values obtained from oceanographic and meteorological ancillary information generally reach the standards adopted in the present study for adequate environmental conditions regarding SAR detection of oil in the sea (**Table 1**). It should be pointed out, however, that on 21 August 2000 QuikSCAT wind speed values ranged from 8.0 to 10.0 $m \cdot s^{-1}$ at the time of RADARSAT-1 acquisition. These high wind speeds did not prevent oil detection in the Cantarell Complex using RADARSAT-1 W1 data. Such a result indicates

that environmental conditions suitable for this application may be in some circumstances extended beyond the upper limit of wind speeds of 8.0 $m \cdot s^{-1}$.

Twenty RADARSAT-1 images in the SCN1, W1, and W2 beam modes were chosen for processing in 2001. After the USTC classification of such a dataset, seepage slicks in the Cantarell area were identified in 19 of the images, as listed in **Table 4**. This demonstrates once again the ability of RADARSAT-1 to remotely detect the presence of generative hydrocarbon source rocks in the southern Gulf of Mexico. The Cantarell seepage slick was not detected only in the RADARSAT-1 W1 image acquired on 13 November 2001 (descending orbit).

In addition, analysis of the 2001 dataset revealed that Cantarell oil seep short-term temporal dynamics could be portrayed whenever possible using two RADARSAT-1 images acquired with subsequent ascending and descending coverage (**Figures 6** and **7**).

Regarding the adequacy of environmental conditions for SAR detection of oil, values obtained from oceanographic and meteorological ancillary information are consistent in most cases with the standards adopted in the present study (**Table 4**). Rain cells situated within the limits of RADARSAT-1 images were observed on several acquisition dates. Fortunately, they were not located in the surroundings of the Cantarell Complex. Reported conditions of weak wind (i.e., wind speed values less than 3.0 $m \cdot s^{-1}$) prevail mostly in sheltered areas along the coast. Therefore, these unfavorable environmental conditions did not hinder oil detection in the Cantarell Complex using RADARSAT-1 data.

Deliverables in this study include thematic maps of natural oil seeps in the Cantarell offshore study area. They refer to the nine W1 images acquired in 2000 (**Figure 8**) and the 19 SCN1, W1, and W2 images acquired in 2001 (**Figure 9**).

Seepage slicks shown in **Figure 8** are situated in the vicinity of the prominent offshore oil seep of the Cantarell Complex. They may be spatially associated with oil pollution from production facilities (see **Figure 5**). However, the fact that these seepage slicks appear in RADARSAT-1 W1 images from nine different acquisition dates strongly validates their authenticity. Therefore, reproducibility in both time and space in the Cantarell Complex is an excellent indication of the existence of these seepage slicks. Similar features in this area were observed in RADARSAT-1 SCN1, W1, and W2 images from 19 different acquisition dates in 2001 (**Figure 9**).

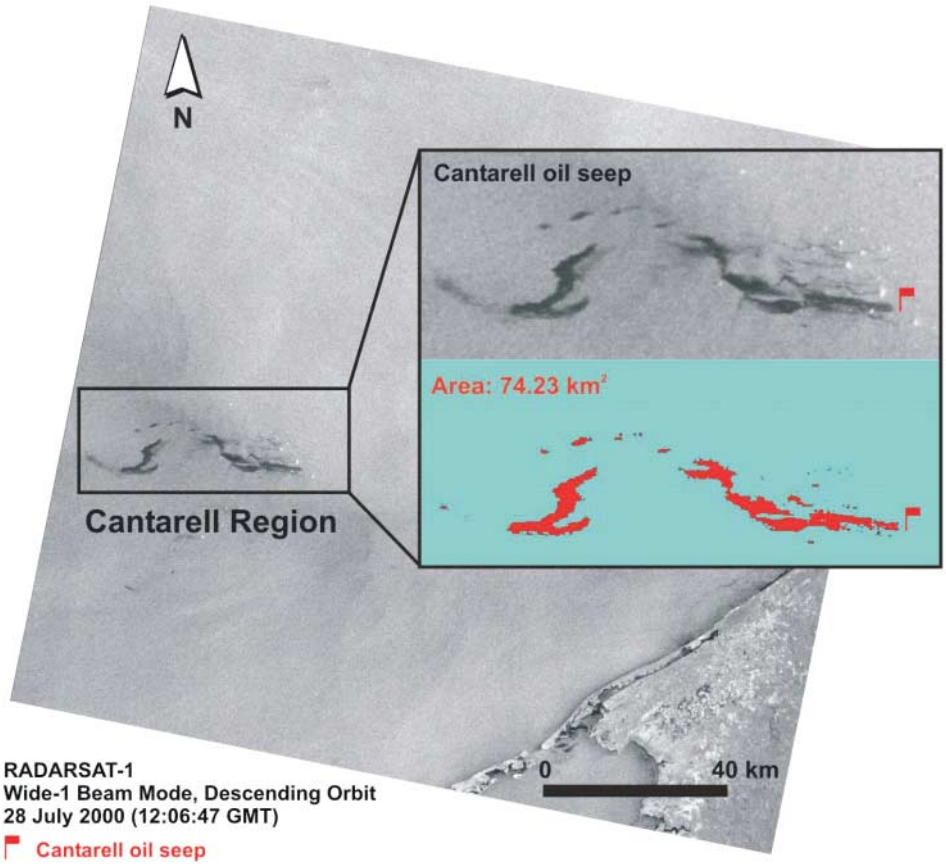

Figure 5. RADARSAT-1 W1 descending image acquired on 28 July 2000, showing the Cantarell seepage slick. Releases of oil from offshore production facilities can also be identified.

Seepage volume estimation from the appearance of oil at sea

As an attempt to assess the oil quantity of the Cantarell seepage activity, we used the Bonn Agreement colour code (Bonn Agreement, 1999). This code is adopted in aerial surveillance campaigns along the North Sea to estimate the volume of observed oil spills (**Table 5**).

According to aerial surveillance campaigns, seepage slicks in the Cantarell Complex can be classified as silvery or rainbow (see **Table 5**). The area occupied by each of the seepage slick polygons is presented in **Tables 6** and **7**. Total amounts of seeped oil calculated using the Bonn Agreement colour code are also shown in these tables. For example, the seepage slick detected using the RADARSAT-1 W1 image acquired on 10 June 2000 has an area of 0.55 km^2 (**Table 6**). Assuming that 100% of this seepage slick is covered by silvery oil,

Table 4. RADARSAT-1 images acquired in 2001 of seepage slicks in the Cantarell area.

Acquisition date (GMT)	Operational beam mode	Orbit	Wind velocity ($m \cdot s^{-1}$)[a]	Wave height (m)[b]	Rain cells[c]
17 Apr.	SCN1	Descending	1.0–6.0	1.0–1.0	Not present
11 May	SCN1	Ascending	3.0–6.0	1.0–1.0	Not present
12 May	SCN1	Descending	7.0–9.0	1.0–1.5	Present
18 May	W1	Ascending	3.0–9.0	1.0–1.0	Not present
11 June	W1	Ascending	3.0–6.0	1.0–1.0	Not present
12 June	SCN1	Descending	2.5–7.0	1.2–1.4	Not present
22 June	W1	Descending	3.0–7.0	0.5–1.0	Not present
28 June	SCN1	Ascending	4.0–9.5	1.3–1.6	Present
06 July	SCN1	Descending	5.0–9.0	0.9–1.2	Not present
22 July	SCN1	Ascending	1.5–9.0	0.4–1.0	Present
23 July	SCN1	Descending	1.0–4.5	0.8–1.2	Not present
09 Aug.	SCN1	Descending	4.0–8.0	1.0–1.4	Present
15 Aug.	SCN1	Ascending	4.0–8.0	0.5–1.0	Not present
08 Sept.	SCN1	Ascending	2.5–9.5	0.5–1.7	Present
15 Sept.	W1	Ascending	4.0–7.0	0.8–1.5	Not present
03 Oct.	SCN1	Descending	3.0–7.5	1.0–1.5	Not present
26 Oct.	SCN1	Ascending	3.0–8.5	1.0–1.3	Present
20 Nov.	SCN1	Descending	2.5–5.0	0.7–2.5	Not present
06 Dec.	W2	Ascending	4.5–7.0	1.3–1.7	Not present

Note: GMT, Greenwich Meridian Time.
[a]QuikSCAT.
[b]TOPEX-Poseidon.
[c]GOES-8.

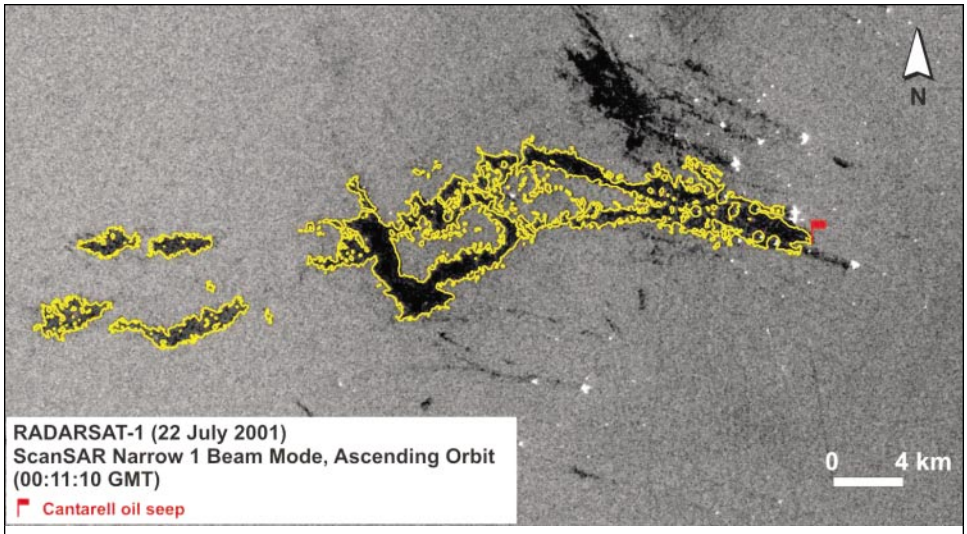

Figure 6. RADARSAT-1 SCN1 ascending image acquired on 22 July 2001, showing the Cantarell seepage slick (highlighted in yellow). Releases of oil from offshore production facilities and local dark features caused by low wind velocities can also be identified.

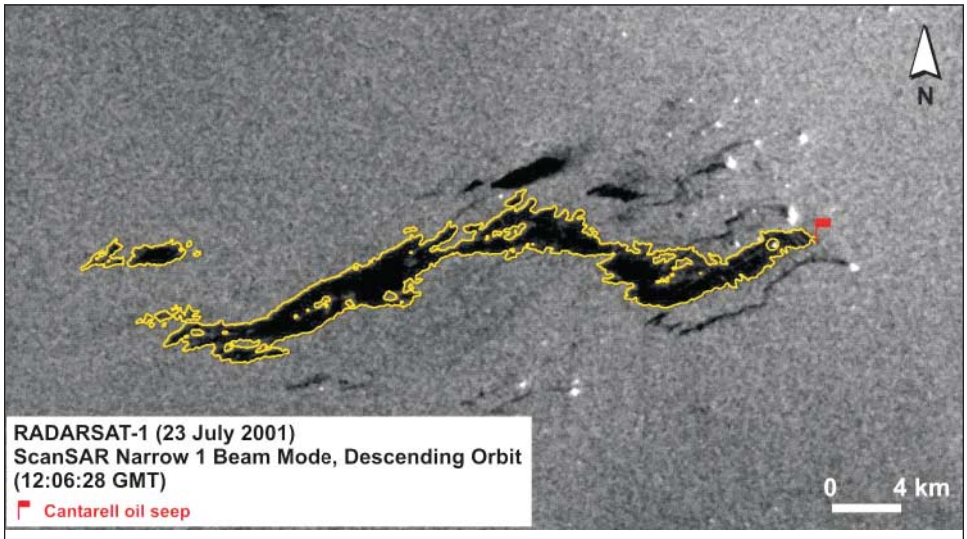

Figure 7. RADARSAT-1 SCN1 descending image acquired on 23 July 2001, showing the Cantarell seepage slick (highlighted in yellow). Releases of oil from offshore production facilities can also be identified.

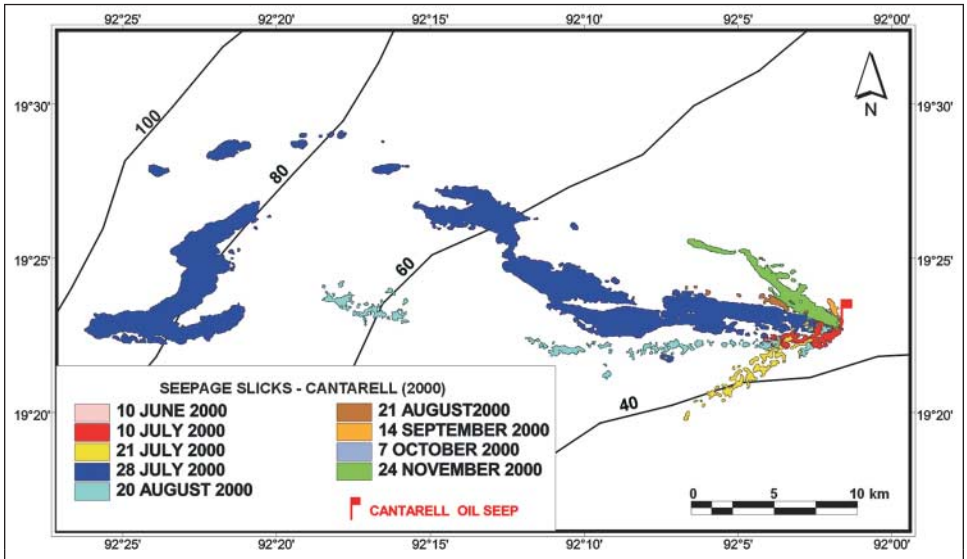

Figure 8. Cantarell seepage slicks identified using RADARSAT-1 W1 images acquired in 2000. Refer to **Figures 1**, **2**, and **3** for location. Contours are labelled in metres.

multiplication of 0.55 km^2 by the color code quantity pertaining to silvery oil (i.e., 0.02 m^3/km^2) gives a total of 0.0110 m^3 seeped. Furthermore, assuming that 100% of this seepage slick is covered by rainbow oil, multiplication of 0.55 km^2 by the color code quantity pertaining to rainbow oil (0.3 m^3/km^2) gives a total of 0.1650 m^3 seeped.

The mean value for polygon areas of **Tables 6** and **7** is 29.0503 km^2, with maximum and minimum values of 0.04 and 154.68 km^2; the mean volume for silvery seeped oil is 0.5810 m^3, with maximum and minimum values of 3.0936 and 0.0008 m^3; and the mean volume for rainbow seeped oil is 8.7151 m^3, with maximum and minimum values of 46.4040 and 0.0120 m^3. Therefore, the results of this study demonstrate that seepage accounts for a substantial portion of oil in the marine environment of southern Gulf of Mexico. Indirect volume estimation from the appearance of seeped oil at sea indicates quantities as high as 46.4040 m^3 (291.87 barrels).

Use of RADARSAT-2 for Cantarell monitoring

RADARSAT-1 beam modes provided by RADARSAT-2 will ensure data continuity of the current oil seep monitoring program in the Cantarell Complex. In addition, RADARSAT-2 and RADARSAT-1 will be offset in time, but otherwise maintaining the same orbit characteristics. Operating in a sun-

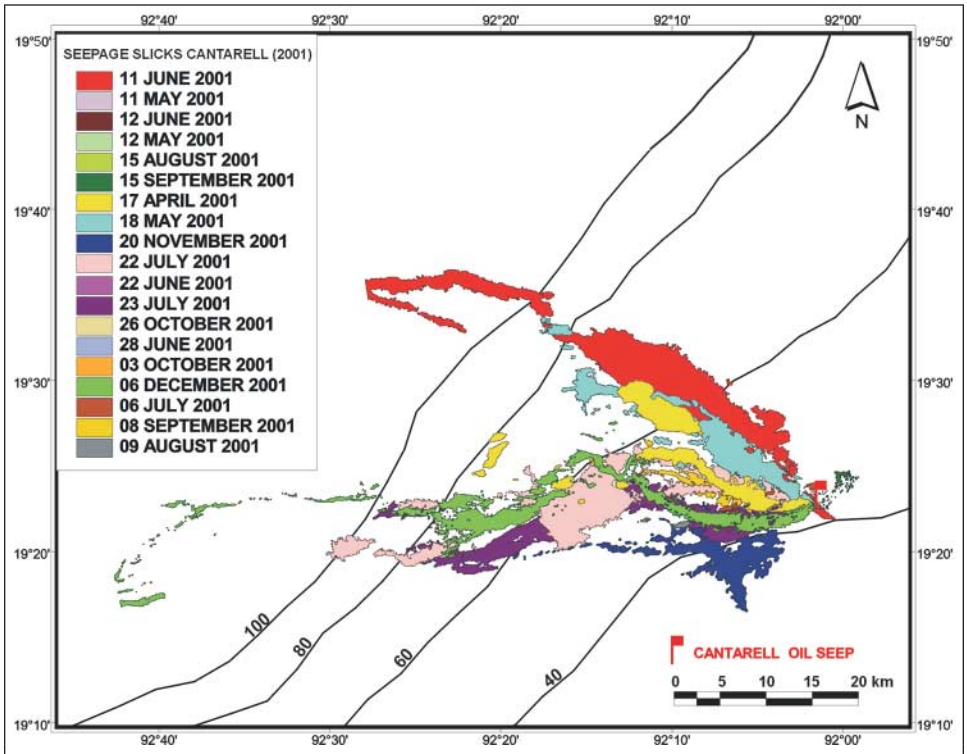

Figure 9. Cantarell seepage slicks identified using RADARSAT-1 SCN1, W1, and W2 images acquired in 2001. Refer to **Figures 1**, **2**, and **3** for location.

Table 5. Estimation of quantity from the appearance of oil at sea (Bonn Agreement, 1999).

Colour code	Quantity (m^3/km^2)
Silvery	0.02
Grey	0.1
Rainbow	0.3
Blue	1
Blue/brown	5
Brown/black	15/25
Dark brown/black	>100

Table 6. Volume estimation for seepage slicks in the Cantarell Complex based on the Bonn Agreement (1999) colour code (RADARSAT-1 W1 images acquired in 2000).

Acquisition date (GMT)	Polygon area (km^2)	Volume estimation (m^3)	
		Silvery	Rainbow
10 June	0.55	0.0110	0.1650
10 July	2.21	0.0442	0.6630
21 July	4.96	0.0992	1.4880
28 July	74.23	1.4846	22.2690
20 Aug.	7.30	0.1460	2.1900
21 Aug.	1.52	0.0304	0.4560
14 Sept.	0.71	0.0142	0.2130
07 Oct.	1.41	0.0282	0.4230
24 Nov.	5.96	0.1192	1.7880

synchronous orbit, both satellites will pass over Cantarell at the same local sun time.

RADARSAT-2 will be able to acquire images either to the right or to the left of the subsatellite track. Such a capability to image on either side of the subsatellite track will shorten the response time and increase the revisit frequency in the Gulf of Mexico. Enhancements in terms of response and revisit times will be particularly valuable to emergency management applications related to oil spills.

The RADARSAT-2 capability to image large areas using VV polarization will enhance its potential for the detection of oil on the ocean surface. In addition, studies carried out by Fortuny-Guasch (2003) suggest that quad-polarized data may provide improved oil detection in the offshore environment.

Conclusions and recommendations

Systematic RADARSAT-1 oil seep detection studies elsewhere in the southern Gulf of Mexico can reveal the presence of unreported regional trends of active petroleum systems. The existence of seepage slicks can be regarded as a positive indicator of hydrocarbon migration, thereby reducing the geologic risk in such an exploration frontier. Acquisition of sea-bottom cores is an independent means to confirm that the slicks are indeed related to seepage phenomena.

Seepage slicks in the Cantarell Complex are spatially associated with oil pollution from production and transportation facilities. However, the fact that these seepage

Table 7. Volume estimation for seepage slicks in the Cantarell Complex based on the Bonn Agreement (1999) colour code (RADARSAT-1 SCN1, W1, and W2 images acquired in 2001).

Acquisition date (GMT)	Polygon area (km^2)	Volume estimation (m^3)	
		Silvery	Rainbow
17 Apr.	57.92	1.1584	17.3760
11 May	2.03	0.0406	0.6090
12 May	2.36	0.0472	0.7080
18 May	67.55	1.3510	20.2650
11 June	154.68	3.0936	46.4040
12 June	0.89	0.0178	0.2670
22 June	0.04	0.0008	0.0120
28 June	2.90	0.0580	0.8700
06 July	3.00	0.0600	0.9000
22 July	132.00	2.6400	39.6000
23 July	96.10	1.9220	28.8300
09 Aug.	11.67	0.2334	3.5010
15 Aug.	2.48	0.0496	0.7440
08 Sept.	27.29	0.5458	8.1870
15 Sept.	2.87	0.0574	0.8610
03 Oct.	8.59	0.1718	2.5770
26 Oct.	1.18	0.0236	0.3540
20 Nov.	63.16	1.2632	18.9480
06 Dec.	77.85	1.5570	23.3550

slicks appear in RADARSAT-1 images from different acquisition dates strongly validates their authenticity. Therefore, reproducibility in both time and space in the area occupied by the *chapopoteras* is an excellent indication of the existence of these seepage slicks.

Despite the reported cases of spills in the Campeche Complex (as depicted in **Figures 5**, **6**, and **7**), it has been verified that a substantial portion of oil in the region originates from natural seeps. Indirect volume estimation from the appearance of seeped oil at sea indicates quantities as high as 46.4040 m^3 (291.87 barrels). Following the demonstration results and field experiments carried out as part of this study, a routine oil seep and oil spill monitoring procedure based on RADARSAT-1 data has been established in Campeche Bay. This initiative will greatly enhance the environmental monitoring capabilities of PEMEX Exploración y Producción.

The USTC textural classification algorithm provided effective enhancement of ocean surface features related to seepage slicks using mainly SCN1 and W1 RADARSAT-1 images. Measurements from the AVHRR NOAA, SeaWinds QuikSCAT, and TOPEX-Poseidon systems were successfully used to provide information about the environmental conditions at the time of RADARSAT-1 data acquisition.

Monitoring of oil spills in the marine environment can be facilitated by the use of spaceborne SAR systems. The experiment with a controlled spill performed in the Gulf of Mexico using an ascending RADARSAT-1 W1 image demonstrated (*i*) the ability of this radar system to detect sea surface oil slicks, and (*ii*) the effectiveness of the textural classification of SAR data based on semivariograms.

Users are encouraged to adopt the methodology described in this paper as a reliable, operational, and cost-effective approach for implementation in the initial stages of risky offshore oil activities (with exploration or environmental focus). Future applications will contemplate the combined use of RADARSAT-1, ENVISAT, and RADARSAT-2 imagery. Such a multisensor microwave dataset will improve the revisit frequency of critical offshore production areas. This will amount up to three images per day in the southern Gulf of Mexico. Furthermore, enhanced polarimetric capabilities may provide improved oil detection in this offshore environment.

Acknowledgements

The authors wish to thank PEMEX Exploración y Producción (PEP) for their generous support in the preparation of the study and for permission to publish the final results. This study is part of a commercial contract between PEP and RSI and an excellent example of the positive outcome that can result from a commercial, technical, and scientific collaboration between committed partners. The reviewer is thanked for comments leading to improvements in the text and tables.

References

Beisl, C.H., Silva, C.L., Jr., and Miranda, F.P. 2000. Combined use of RADARSAT-1 and AVHRR data for the identification of mesoscale oceanic features in the Campos Basin, Brazil. In *Proceedings of the 6th International Conference on Remote Sensing for Marine and Coastal Environments*, 1–3 May 2000, Charleston, S.C. Environmental Research Institute of Michigan (ERIM) (now Altarum), Ann Arbor, Mich. Vol. 2, pp. 415–420.

Bentz, C.M., and Miranda, F.P. 2001. Application of remote sensing data for oil spill monitoring in the Guanabara Bay, Rio de Janeiro, Brazil. In *IGARSS'01, Proceedings of the International Geoscience and Remote Sensing Symposium*, 9–13 July 2001, Sydney, Australia. IEEE, New York [CD-ROM].

Bentz, C.M., Miranda, F.P., Pedroso, E.C., and Beisl, C.H., 2000, Application of remote sensing data for oil spill monitoring in the Guanabara Bay, Rio de Janeiro, Brazil: preliminary results. In *Proceedings of the 7th Latin-American Congress on Organic Geochemistry*, 22–26 Oct. 2000, Foz do Iguaçu, Brazil. ALAGO Congress Secretariat, Petrobras, Rio de Janeiro, Brazil [CD-ROM].

Biegert, E.K., Baker, R.N., Berry, J.L., Mott, S., and Scantland, S. 1997. Gulf Offshore Satellite Applications Project detects oil slicks using RADARSAT. In *Geomatics in the Era of RADARSAT (GER'97), Proceedings of the 13th International Symposium*, 26–30 May 1997, Ottawa, Ont. Geomatics Canada, Natural Resources Canada. [CD-ROM].

Bonn Agreement. 1999. *Bonn Agreement counter pollution manual*. Vol. 1, Chapt. 4, Annex 1. Available from http://www.bonnagreement.org/eng/html/counter-pollution_manual [accessed on 24 April 2002].

Carr, J.R. 1996. Spectral and textural classification of single and multiple band digital images. *Computers and Geosciences*, Vol. 22, pp. 849–866.

Carr, J.R., and Miranda, F.P. 1998. The semivariogram in comparison to the co-occurrence matrix for classification of image texture. *IEEE Transactions on Geoscience and Remote Sensing*, Vol. 36, pp. 1945–1952.

Espedal, H.A., and Johannessen, O.M. 2000. Detection of oil spills near offshore installations using synthetic aperture radar (SAR). *International Journal of Remote Sensing*, Vol. 21, pp. 2141–2144.

Fingas, M., and Brown, C. 1997. Remote sensing of oil spills. *Sea Technology*, Vol. 38, pp. 37–46.

Fonseca, L.E.N. 1996. Radiometric corrections of Campos Basin side scan sonar data. In *Proceedings of the 8th Brazilian Symposium of Remote Sensing*, June 1996, Santos, Brazil. INPE, São José dos Campos, São Paulo, Brazil [CD-ROM].

Fortuny-Guasch, J. 2003. Improved oil slick detection and classification with polarimetric SAR. In *POLinSAR 2003, Proceedings of the Workshop on Application of SAR Polarimetry and Polarimetric Interferometry*, 14–16 Jan. 2003, Frascati, Italy. POLINSAR Proceedings SP-529, European Space Agency (ESA) Publications Division, Noordwijk, The Netherlands [CD-ROM].

Fu, L.L., and Holt, B. 1982. *Seasat views oceans and sea ice with synthetic aperture radar.* Jet Propulsion Laboratory, Pasadena, Calif., JPL Publication 81-120. 200 pp.

Johannessen, J.A., Digranes, G., Espedal, H., Johannessen, O.M., Samuel, P., Browne, D., and Vachon, P.W. 1994. *SAR ocean feature catalogue*. European Space Agency (ESA) Publications Division, Noordwijk, The Netherlands, ESA SP-1174. 106 pp.

MacDonald, J.A. 1991. *Automatic classification of satellite images in the textural domain using semivariograms*. M.Sc. dissertation, University of Nevada, Reno, Nev. 82 pp.

MacDonald, I.R., Reilly, J.F., Jr., Best, S.E., Venkataramaiah, R., Sassen, R., Guinasso, N.L., Jr., and Amos, J. 1996. Remote sensing inventory of active oil seeps and chemosynthetic communities in the northern Gulf of Mexico. In *Hydrocarbon migration and its near-surface expression*. Edited by D. Schumaker and M.A. Abrams. American Association of Petroleum Geologists, Tulsa, Okla. AAPG Memoir 66, pp. 27–37.

Miranda, F.P. 1990. *Reconnaissance geologic mapping of a heavily-forested shield area (Guiana Shield, northwestern Brazil)*. Ph.D. thesis, University of Nevada, Reno, Nev. 176 pp.

Miranda, F.P., and Carr, J.R. 1994. Application of the semivariogram textural classifier (STC) for vegetation discrimination using SIR-B data of the Guiana Shield, northwestern Brazil. *Remote Sensing Reviews*, Vol. 10, pp. 155–168.

Miranda, F.P., and MacDonald, J.A. 1989. A variogram study of SIR-B data in the Guiana Shield, Brazil. In *Proceedings of the Image Processing '89 Conference*, 23–26 May 1989, Reno, Nev. pp. 66–77.

Miranda, F.P., MacDonald, J.A., and Carr, J.R. 1992. Application of the semivariogram textural classifier (STC) for vegetation discrimination using SIR-B data of Borneo. *International Journal of Remote Sensing*, Vol. 13, pp. 2349–2354.

Miranda, F.P., Fonseca, L.E.N., Carr, J.R., and Taranik, J.V. 1996. Analysis of JERS-1 (Fuyo-1) SAR data for vegetation discrimination in northwestern Brazil using the semivariogram textural classifier (STC). *International Journal of Remote Sensing*, Vol. 17, pp. 3523–3529.

Miranda, F.P., Fonseca, L.E.N., Beisl, C.H., Rosenqvist, A., and Figueiredo, M.D.M.A.M. 1997. Seasonal mapping of flooding extent in the vicinity of the Balbina Dam (Central Amazonia) using RADARSAT-1 and JERS-1 SAR data. In *Geomatics in the Era of RADARSAT (GER'97), Proceedings of the 13th International Symposium*, 26–30 May 1997, Ottawa, Ont. Geomatics Canada, Natural Resources Canada [CD-ROM].

Miranda, F.P., Fonseca, L.E.N., and Carr, J.R. 1998a. Semivariogram textural classification of JERS-1 (Fuyo-1) SAR data obtained over a flooded area of the Amazon rainforest. *International Journal of Remote Sensing*, Vol. 19, pp. 549–556.

Miranda, F.P., Bentz, C.M., Beisl, C.H., Lorenzzetti, J.A., Araújo, C.E.S., and Silva, C.L., Jr. 1998b. Application of unsupervised semivariogram textural classification of RADARSAT-1 data for the detection of natural oil seeps offshore the Amazon River mouth. In *Proceedings of the RADARSAT ADRO Symposium*, 13–15 Oct. 1998, Montréal, Que. [CD-ROM].

Miranda, F.P., Bentz, C.M., Beisl, C.H., Lorenzzetti, J.A., Araújo, C.E.S., and Silva, C.L., Jr. 1998c. Oil seep detection using RADARSAT-1 data in offshore frontier areas of northern Brazil. In *Proceedings of the 6th Latin American Congress on Organic Geochemistry*, Oct. 1998, Margarita Island, Venezuela. ALAGO Congress Secretariat, Petrobras, Rio de Janeiro, Brazil [CD-ROM].

Miranda, F.P., Bentz, C.M., Beisl, C.H., Lorenzzetti, J.A., Araújo, C.E.S., and Silva, C.L., Jr. 1998d. Application of the unsupervised semivariogram textural classifier (USTC) for the detection of natural oil seeps using RADARSAT-1 data obtained offshore the Amazon River mouth, Brazil. In *Extended Abstracts Volume of the 1998 AAPG International Conference & Exhibition*, 8–11 Nov. 1998, Rio de Janeiro, Brazil. pp. 198–199.

Rubin, T. 1989. Analysis of radar image texture with variograms and other simplified descriptors. In *Proceedings of the Image Processing '89 Conference*, 23–26 May 1989, Reno, Nev. pp. 185–195.

Scantland, S., and Biegert, E.K. 1996. Radar locates offshore oil slicks. *Earth Observation Magazine*, Vol. 5, pp. 30–32.

Staples, G.C, and Hodgins, D.O. 1998. RADARSAT-1 emergency response for oil spill monitoring. In *Proceedings of the 5th International Conference on Remote Sensing for Marine and Coastal Environments*, 5–7 Oct. 1998, San Diego, Calif. Environmental Research Institute of Michigan (ERIM) (now Altarum), Ann Arbor, Mich.